How to cite: *Angew. Chem. Int. Ed.* **2022,** *61,* e202212473
International Edition: doi.org/10.1002/anie.202212473
German Edition: doi.org/10.1002/ange.202212473

Molecular Devices

Synchronizing Two Distinct Nano-Circular Sliding Motions in Six-Component Machinery for Double Catalysis

*Vishnu Verman Rajasekaran, Amit Ghosh, Sohom Kundu, Debabrata Mondal, Thomas Paululat, and Michael Schmittel**

Dedicated to Professor Hiriyakkanavar Ila

Abstract: The heteroleptic multi-component double slider-on-deck system **DS3** exhibits tight coupling of motional speed of two distinct nano-circular sliders (k_{298} = 77 and 41 kHz) despite a 2.2 nm separation. In comparison, the single sliders in **DS1** and **DS2** move at vastly different speed (k_{298} = 1.1 vs. 350 kHz). Synchronization of the motions in **DS3** remains even when one slows the movement of the faster slider using small molecular brake pads. In contrast to the individual **DS1** and **DS2** systems, **DS3** is a powerful catalyst for a two-step reaction by using the motion of both sliders to drive two catalytic processes.

Synchronized motion in machines plays a ubiquitous role in nature to maintain life[1] by acting as energy transducer,[2] e.g. in the synthesis of ATP as a high-energy product and fuel by the multi-component F_oF_1-ATP synthase. Via efficient intercomponent communication, conformational changes in the F_o subunit lead to cyclic structural changes in the F_1 unit which mediate a phase-shifted conversion of ADP and P_i to ATP.[3]

While motional speed in artificial machines has been a topic of great interest,[4–9] lately even in combination with catalysis,[10–13] we decided to pursue the concept of synchronized movement[14,15] in catalytic multicomponent machinery alike that in enzymes. Coupling of motion in individual self-assembled machines with multiple moving parts is very rarely reported,[16–18] and even less regarding distinct catalytic behavior.[19] Mostly coupling is achieved by geared motion in molecular arrangements.[20,21] Hence, the challenge to synchronize motion in a self-assembled multi-component machine and to exploit the coupled movement for double catalysis remains unexplored.

Here, we report on three slider-on-deck systems, **DS1–DS3**, that are readily assembled using orthogonal interactions[22] and self-sorting (HETPYP, N_{py}→ZnPor and homoleptic[23] $[Zn(terpy)_2]^{2+}$ {terpy = 2,2′:6′, 2″-terpyridine} complexations, see Figure 1) to enable two sliding motions with distinct exchange rates. Lastly, we will couple two catalytic functions to the stochastic motion of the slider-on-deck **DS3**.

Mixing ligands **1**, **2** and $[Cu(MeCN)_4]^+$ (Figure 1) in a 1:1:3 ratio quantitively assembled the three-component HETPYP slider-on-deck **DS1** (Figure 2), which was fully characterized by spectroscopic data (^{1}H, ^{1}H-^{1}H COSY, ^{1}H DOSY, ESI-MS) and elemental analysis. Figure 3a–c shows the pronounced ^{1}H NMR changes that accompany the formation of **DS1** from its respective components. The binding and sliding motion of the lutidine terminals of **2** across the $[Cu_3(\mathbf{1})]^{3+}$ unit causes drastic shifts and broadening of the proton signals i,p-H from 7.05 ppm in **1** to 6.65 and 6.85 ppm in **DS1**. Similarly, notable shifts and broadening of signals k,n-H located on the diarylphenanthroline unit from 7.97–7.99 ppm in deck **1** to 8.85 and 8.22 ppm and the emergence of the f′-H signal at 2.07 ppm in **DS1** (2.54 ppm in free **2**) corroborate the assembly formation. Broadening of NMR signals suggests dynamic sliding in **DS1**, for instance, by the circular motion of **2** between three degenerate $[Cu(phenAr_2)]^+$ units on **1**.

Analogously, the slider-on-deck **DS2** was assembled by mixing ligand **1** and the homoleptic bis-terpyridine complex $[Zn(\mathbf{3})_2]^{2+}$ (1:1). Formation of **DS2** was ascertained by spectroscopic methods (^{1}H, ^{1}H-^{1}H COSY, ^{1}H DOSY NMR) and elemental analysis. The large upfield shift of β″-H from 7.42 ppm in $[Zn(\mathbf{3})_2]^{2+}$ to 5.67 ppm in **DS2** along with the upfield shift of the r-H signal from 10.34 ppm in **1** to 10.25 ppm in **DS2** were both attributed to the axial N_{py}→ZnPor coordination (Figure 3c–e) exchanging between all three ZnPor sites.

After preparing the individual slider-on-deck systems **DS1** and **DS2**, we assembled the double slider-on-deck **DS3** by mixing **1**, **2**, Cu^+, $[Zn(\mathbf{3})_2]^{2+}$ in a 1:1:3:1 ratio. Quantitative formation of **DS3** was confirmed by spectroscopic data (^{1}H, ^{1}H-^{1}H COSY, ^{1}H DOSY NMR) and

[*] V. V. Rajasekaran, Dr. A. Ghosh, S. Kundu, D. Mondal, Prof. Dr. M. Schmittel
Center of Micro and Nanochemistry and (Bio)Technology, Organische Chemie I, University of Siegen
Adolf-Reichwein Str. 2, 57068 Siegen (Germany)
E-mail: schmittel@chemie.uni-siegen.de
Dr. T. Paululat
Center of Micro and Nanochemistry and (Bio)Technology, Organische Chemie II, University of Siegen
Adolf-Reichwein Str. 2, 57068 Siegen (Germany)

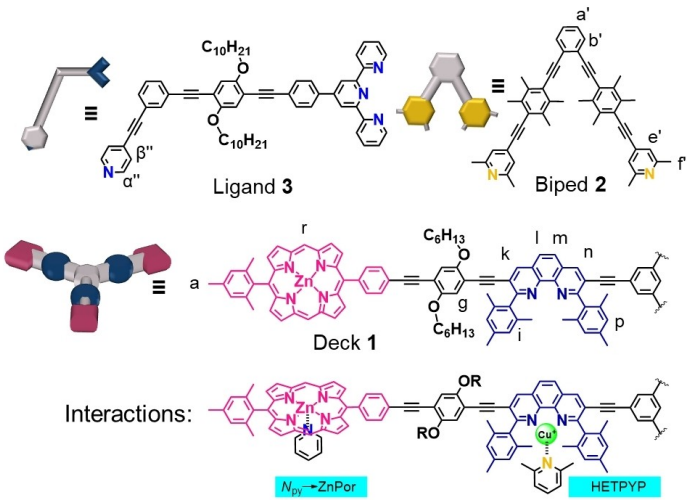

Figure 1. Ligands and interactions[24,25] used in this study.

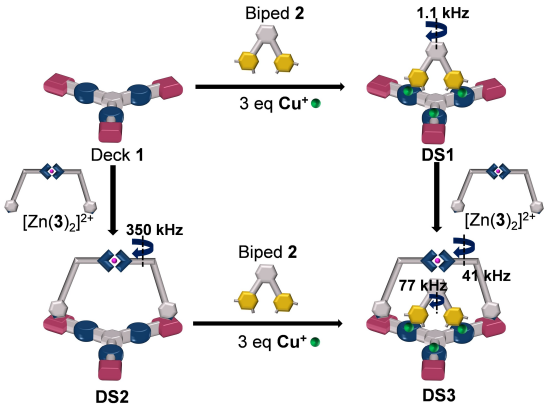

Figure 2. Stepwise conversion between the HETPYP slider-on-deck **DS1**, N_{py}→ZnPor slider-on-deck **DS2** and double slider-on-deck **DS3**.

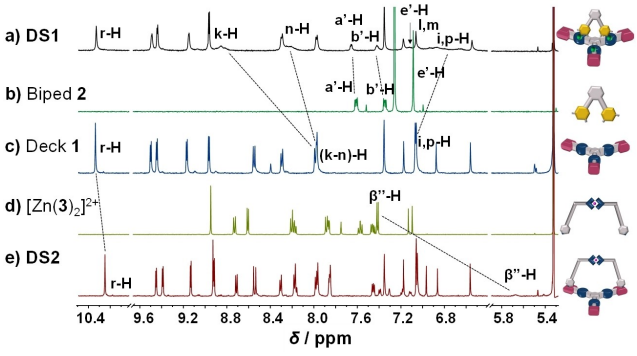

Figure 3. Comparison of partial ^{1}H NMR (500 MHz, CD_2Cl_2, 298 K) spectra of a) slider-on-deck **DS1** = $[Cu_3(\mathbf{1})(\mathbf{2})]^{3+}$, b) free biped **2** in $CDCl_3$, c) free deck **1**, d) $[Zn(\mathbf{3})_2]^{2+}$, and e) the N_{py}→ZnPor slider-on-deck **DS2** = **1**·$[Zn(\mathbf{3})_2]^{2+}$.

elemental analysis. A comparison of **DS3** with **DS1** and **DS2** indicated that both dynamic interactions, i.e., HETPYP and N_{py}→ZnPor, were preserved in **DS3**. Further, all three assemblies **DS1-DS3** were characterized by their diffusion coefficients (r_s (**DS1**) = 14.5 Å, r_s (**DS2**) = 15.5 Å, r_s (**DS3**) = 13.7 Å) obtained from DOSY NMR experiments confirming their quantitative formation (Supporting Information, Figure S26–S28).

To quantify the sliding dynamics, we undertook variable temperature (VT) ^{1}H NMR studies that confirmed the dynamic coordination of both lutidine terminals of biped **2** to all three degenerate $[Cu(phenAr_2)]^+$ stations of deck **1**. The g-H proton of **1** in **DS1** was chosen as the diagnostic signal because at 298 K it appears as a sharp singlet (6.54 ppm) and separates at 243 K into two singlets (1:2) at 6.46 and 6.41 ppm. The signal at 6.41 ppm is assigned to phenyl protons g-H at lutidine-coordinated $[Cu(phenAr_2)]^+$ units, whereas the broader signal at 6.46 ppm represents the g-H signal of the freely rotating phenyl ring adjacent to the vacant $[Cu(phenAr_2)]^+$ site. A kinetic analysis provided the exchange frequency (k) of the sliding motion at various temperatures (Figure 4a) as $k_{298} = 1.1 \times 10^3\ s^{-1}$ (at 298 K). Activation parameters are $\Delta H^{\neq} = 66.5 \pm 1.1\ kJ\,mol^{-1}$ and $\Delta S^{\neq} = 36.3 \pm 4.0\ J\,mol^{-1}K^{-1}$ furnishing a free activation energy for exchange at 298 K as $\Delta G^{\neq}_{298} = 55.7 \pm 2.3\ kJ\,mol^{-1}$.

Additionally, we recorded the VT ^{1}H NMR of **DS2** that confirmed the dynamic coordination of the two pyridine terminals of the di-topic biped $[Zn(\mathbf{3})_2]^{2+}$ to the three

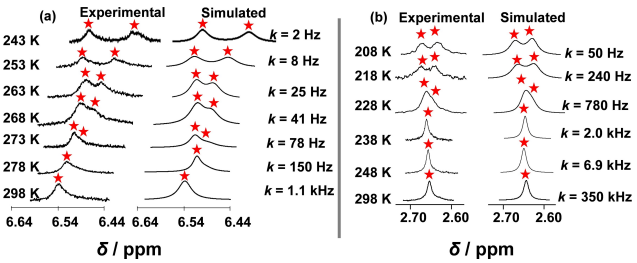

Figure 4. Experimental and theoretical splitting in VT ^{1}H NMR spectra (600 MHz). Proton a) g-H signal of slider-on-deck **DS1** and b) a-H signal of **DS2** in CD_2Cl_2 furnishing rate data at different temperatures.

degenerate zinc porphyrins in **DS2**. The proton signal a-H of the porphyrin nucleus was chosen because its sharp singlet at 298 K separated at 208 K into two broad singlets (2:1) at 2.66 and 2.62 ppm. While the signal at 2.62 ppm corresponds to the pyridine-coordinated zinc porphyrins, the freely rotating third porphyrin furnishes a broader signal at 2.66 ppm. A kinetic analysis provides the frequency (k) for sliding (Figure 4b) with $k_{298} = 3.5 \times 10^5\ s^{-1}$ and the activation parameters $\Delta H^{\ddagger} = 48.2 \pm 0.9\ kJ\,mol^{-1}$, $\Delta S^{\ddagger} = 23.3 \pm 3.8\ J\,mol^{-1}\,K^{-1}$ as well as $\Delta G^{\ddagger}_{298} = 41.2 \pm 2.0\ kJ\,mol^{-1}$.

Subsequently, we also recorded the VT ^{1}H NMR of **DS3** to study the two orthogonal dynamic motions on deck **1**. The proton r-H signal of the zinc porphyrin showed a sharp singlet at 298 K but split at 243 K into two singlets (2:1) at 10.28 and 10.24 ppm (Supporting Information, Figures S33–S35). Whereas the signal at 10.28 ppm corresponds to the pyridine-coordinated zinc porphyrins, the freely rotating third porphyrin exhibits a broader signal at 10.24 ppm. A kinetic analysis provided $k_{298} = 4.1 \times 10^4\ s^{-1}$ for the $N_{py}\rightarrow$ ZnPor sliding along with the activation parameters $\Delta H^{\ddagger} = 49.6 \pm 0.4\ kJ\,mol^{-1}$, $\Delta S^{\ddagger} = 9.4 \pm 1.9\ J\,mol^{-1}\,K^{-1}$ and $\Delta G^{\ddagger}_{298} = 46.8 \pm 1.0\ kJ\,mol^{-1}$. To quantify in the same VT ^{1}H NMR spectra the $N_{lut}\rightarrow[Cu(phenAr_2)]^+$ (HETPYP) dynamics of **DS3** we focused on proton g-H, since its sharp singlet (at 298 K) separated at 218 K into two broad singlets (2:1) at 6.31 and 6.34 ppm. While the signal at 6.31 ppm corresponds to the two lutidine-coordinated $[Cu(phenAr_2)]^+$ stations, the freely rotating $[Cu(phenAr_2)]^+$ furnishes a broader signal at 6.34 ppm. The kinetic analysis provided k_{298} ($N_{lut}\rightarrow[Cu(phenAr_2)]^+$) $= 7.7 \times 10^4\ s^{-1}$ along with the activation parameters $\Delta H^{\ddagger} = 46.2 \pm 0.4\ kJ\,mol^{-1}$, $\Delta S^{\ddagger} = 4.2 \pm 1.6\ J\,mol^{-1}\,K^{-1}$ and $\Delta G^{\ddagger}_{298} = 45.0 \pm 0.8\ kJ\,mol^{-1}$ (Table 1).

Notably, the above kinetic analysis of the dual slider-on-deck **DS3** (Table 1) suggests that the $N_{py}\rightarrow$ZnPor binding of biped $[Zn(\mathbf{3})_2]^{2+}$ is enhanced at the cost of the $N_{lut}\rightarrow[Cu(phenAr_2)]^+$ binding of biped **2**. Most surprising is the drastic increase of the exchange frequency for the lutidine biped from $k_{298} = 1.1$ kHz in **DS1** to $k_{298} = 77$ kHz in **DS3** accompanied by a drastic decrease in the exchange rate of the pyridine biped from $k_{298} = 350$ kHz in **DS1** to $k_{298} = 41$ kHz in **DS3** (Table 1). The close matching of both frequencies suggests that a single event determines the rates. To check whether the $N_{lut}\rightarrow [Cu(phenAr_2)]^+$ dissociation is rate-limiting, we slowed the motion of the lutidine slider of **DS3** applying small molecular brake pads, namely 5-bromo-2-pyridine carboxaldehyde and 2-pyridine carboxamide. Both compounds, if applied in a 1:1 stoichiometry w.r.t **DS3**, should bind as chelate ligands at the free $[Cu(phenAr_2)]^+$ site on **DS3**, requiring that for any motion of the lutidine slider **2** in **DS3** the biped has to kick out the brake pad. The latter will then associate to the newly liberated $[Cu(phenAr_2)]^+$ site slowing again the next motion of the lutidine biped **2**, a concept that has recently been tested in related dynamic slider-on-deck systems.[26] Importantly, if there is no coupling between the two sliding motions in **DS3**, the movement of the pyridine biped should be unaffected.

Accordingly, we assembled **DS3** including the brake pad by mixing **1**, **2**, Cu^+, $[Zn(\mathbf{3})_2]^{2+}$ and the chelate (brake pad) in a 1:1:3:1:1 ratio. The **DS3** assemblies including 5-bromo-2-pyridine carboxaldehyde and 2-pyridine carboxamide will be hereafter referred to as **DS3′** and **DS3″**, respectively. VT ^{1}H NMR investigations and subsequent kinetic analyses were performed for **DS3′** and **DS3″** as described previously. Table 1 summarizes the activation parameters and rate data for each individual slider-on-deck system.

Upon inspection of the data in Table 1 we see several mechanistically surprising trends. Firstly, the exchange frequencies k_{lut} and k_{py} in **DS3**, **DS3′** and **DS3″** merge in between 1.1 kHz (as in **DS1**) and 350 kHz (as in **DS2**) with the numbers slightly declining upon addition of the brake pads. Such a finding suggests that there must be strong strain effects in **DS3** (despite a 2.2 nm separation of the bipeds, Supporting Information, Chapter 7) that reduce k_{py} and increase k_{lut}.[27] Secondly, the lutidine slider, which is extremely slow in **DS1**, is accelerated by more than 60-fold in **DS3** and is now the faster process ($k_{lut} > k_{py}$). Thirdly, the ratio of the k_{lut}/k_{py} in **DS3**, **DS3′** and **DS3″** is approximately constant, roughly by a factor of 2, as also reflected by a constant increment $\Delta\Delta G^{\ddagger}_{298} = 1.9\ kJ\,mol^{-1}$ for the two free energy activation barriers in **DS3**, **DS3′** and **DS3″**. A rationalization of the constant increment $\Delta\Delta G^{\ddagger}_{298}$ in **DS3**, **DS3′** and **DS3″** has to consider (a) that both exchange processes have a different rate determining step, although they appear synchronized, and (b) that the rate of the $N_{py}\rightarrow$ ZnPor dissociation must be dictated by the lutidine slider, as the brake pads can only influence the motional speed of the latter.

For a discussion of the mechanism to delineate the cause of the apparent synchronization, we must first identify the global minimum structure(s) of **DS3**. On one hand there is the *anti*-configuration "A" (altogether six degenerate structures) where the bipeds **2** and $[Zn(\mathbf{3})_2]^{2+}$ are connected to different arms of the deck **1** (Figure 5). The notation for any of the *anti*-structures describes the position (i.e. 1, 2 or 3) of biped **2** on deck **1** as the subscript, e.g. in A_1''', and the position (i.e. ′, ″ or ‴) of $[Zn(\mathbf{3})_2]^{2+}$ on deck **1** as the superscript in A_1'''.

Table 1: Summary of activation parameters and kinetic analysis of sliders-on-deck (**DS1**, **DS2**, **DS3**, **DS3′** and **DS3″**) categorized by the two individual rate-determining steps involving $N_{py}\rightarrow$ZnPor and $N_{lut}\rightarrow$-$[Cu(phenAr_2)]^+$ dissociation. **DS3′** = **DS3** + 5-bromo-2-pyridine carboxaldehyde. **DS3″** = **DS3** + 2-pyridine carboxamide.

	Machine	$\Delta H^{\ddagger}$ (kJ•mol^{-1})	$\Delta S^{\ddagger}$ (J•mol^{-1}K^{-1})	$\Delta G^{\ddagger}_{298}$ (kJ•mol^{-1})	k_{298} (kHz)
$N_{py}\rightarrow$ZnPor	**DS1**	na	na	na	na
	DS2	48.2	23.3	41.2	350
	DS3	49.6	9.4	46.8	41
	DS3'	49.1	4.7	47.7	28.7
	DS3"	48.9	2.0	48.4	20

	Machine	$\Delta H^{\ddagger}$ (kJ•mol^{-1})	$\Delta S^{\ddagger}$ (J•mol^{-1}K^{-1})	$\Delta G^{\ddagger}_{298}$ (kJ•mol^{-1})	k_{298} (kHz)
$N_{lut}\rightarrow$ $[Cu(phenAr_2)]^+$	**DS1**	66.5	36.3	55.7	1.1
	DS2	na	na	na	na
	DS3	46.2	4.2	45.0	77
	DS3'	46.5	2.7	45.7	59
	DS3"	47.9	5.3	46.4	42

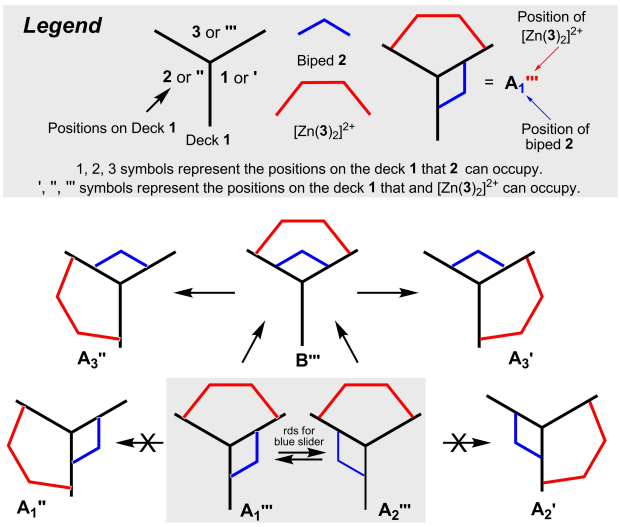

Figure 5. Representation of some degenerate structures A and B formed in the motion of **DS3**. Representative of other degenerate arrangements, the motion will start from A_1''' and A_2'''.

The *syn*-structures B comprise three degenerate structures (B′, B″, B‴) where the bipeds **2** and $[Zn(\mathbf{3})_2]^{2+}$ are connected to the same two arms of deck **1**. Hence the notation (e.g. B′) only requires the specification of the position of one of the two sliders. The legend in Figure 5 describes the notation used for discussions in the succeeding paragraphs.

If we begin by postulating that the *syn*-structures B were the ground state, then any single-step motion of the lutidine slider **2** would inevitably lead to the higher-energy *anti*-structures A, which should not (or hardly) be visible at equilibrium. In such a situation, the NMR would reflect the exchange B‴⇆B′⇆B″, requiring that both individual sliding processes have a single rate-determining step and by extension an identical rate constant for k_{lut} and k_{py}. The experimental data presented in Table 1, however, do not support such model.

Hence, the above experimental findings lead us to postulate that A are the ground-state structures. Suppose the motion starts from A_1''' and A_2''' (Figure 5). Interestingly, any exchange $A_1'''⇆A_2'''$ already allows the lutidine slider to visit all three copper(I) phenanthroline stations. Such process, although it does not involve *syn*-structures B, may appear in the NMR like a full exchange since different positioning of one slider should not impact on the ^{1}H NMR shifts of the other slider due to their large spatial separation (ca. 2.2 nm).

Furthermore, there are a couple of experimental findings that need to be explained in a plausible mechanism after A has been identified as the ground state structure: (a) Since $\Delta\Delta G^{\ddagger}_{298}$ (k_{py} vs k_{lut}) is constant by ca. 2 kJ mol^{-1} in **DS3**, **DS3′** and **DS3″**, the motion of the pyridine biped $A_1'''→A_1''$ or $A_2'''→A_2'$ must be impeded by a high N_{py}→ZnPor dissociation barrier. Otherwise, the pyridine slider would also be able to visit all three ZnPor sites (=full exchange) and furthermore its motion would become independent of the lutidine slider. (b) Consequently, motion of the pyridine slider is only possible in state B‴, which has first to form in an endergonic step from A_1''', A_2''' by lutidine migration. As B‴ is higher in energy and thus more strained than A_1''', A_2''', there is a good rationale why the strain-driven N_{py}→ZnPor dissociation of the pyridine biped in B‴ leading to structures A_3' or A_3'' is now faster than the reverse motion of the lutidine slider. (c) Importantly, such a mechanism readily explains why the motion of the pyridine biped will always depend on the lutidine slider's migration to the higher energy structures B, either with or without the brake pads.

By computation one can test part of this mechanistic scenario, because it predicts that B must be thermodynamically higher in energy than A. Indeed, the computational energy calculations predict that structure A is more stable than B by 26.7 kJ mol^{-1} (Supporting Information, Figure S48–S50). With the computational and experimental data at hand, we are able to sketch the energy profile of the synchronized sliding. From the energy hypersurface, we realize that the process A‴→B‴ is endergonic (e.g. A_2'''→B‴ in Figure 6), which increases the activation free energy of lutidine sliding by $\Delta\Delta G^{\ddagger}_{298}$ = ca. 2 kJ mol^{-1} compared to that for $A_1'''⇆A_2'''$. Assuming that the follow-up motion of the pyridine slider in B is now faster (e.g. B‴→A_3') than the return to any of the two A‴ (e.g. B‴→A_2''') the system progresses to A_3' or A_3'' (Figure 6).

Finally, after rationalizing the synchronization of both sliding exchange processes in **DS3**, we sought for a possibility to use the coupled sliding for a reaction that is promoted by two catalysts. Former work in our group[12,13] had established individual catalytic slider-on-deck systems for both copper(I) phenanthroline (click reaction) and zinc porphyrin systems (catalyst release leading to various organocatalytic reactions), in which catalysis vastly profits from motion.

We thus decided to utilize **DS3** with its ability to liberate an organic tertiary amine (=catalyst 1) from the ZnPor unit due to the motion[12] and the dynamically exposed Cu^+ (=catalyst 2)[13] for a reaction requiring two catalysts. The amine was expected to deprotonate **4** thus facilitating the copper(I)-catalyzed cyclization furnishing **5** (Scheme 1). To test the two-step reaction, we mixed **4** (5.0 mM), 1,3,5-trimethoxybenzene, **DS3**, *N*-methylpyrrolidine (NMP) in a

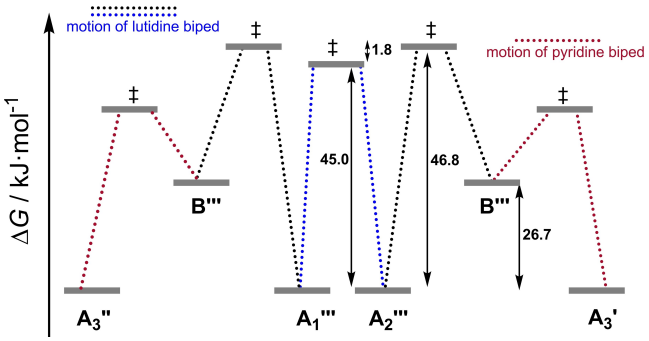

Figure 6. Semiquantitative energy profile for **DS3**.

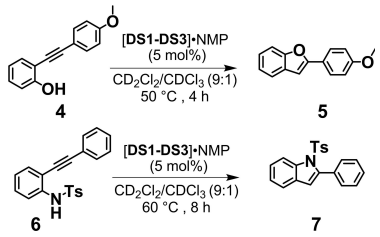

Scheme 1. Catalytic transformation of the reactions **4**→**5** and **6**→**7** using 5 mol% of [**DS1**–**DS3**·NMP]. NMP = *N*-methylpyrrolidine.

20:20:1:1 ratio in CD_2Cl_2:$CDCl_3$ (9:1) in an NMR tube and heated it at 50 °C for 4 h. The resultant mixture was subjected to ^{1}H NMR which revealed 49 % yield of product **5** (Figure 7a). Importantly, reaction **4**→**5** is poorly catalyzed by (**DS1**·NMP) since NMP is rendered mainly inactive due to its binding at the zinc porphyrin units resulting in only 3 % yield of **5**. Use of **DS2** as catalyst expectedly resulted in no yield of **5** at all due to the lack of copper(I).

The methodology has a wide scope as it was readily extended to the catalyzed conversion of **6** to **7** (Scheme 1, Figure 7b). Further, monitoring the kinetics of formation of **5** and **7** in all three sliders (**DS1–DS3**) revealed a v_0(**DS3**)/v_0(**DS1**) = 7.4 for **5** and v_0(**DS3**)/v_0(**DS1**) = 20.3 for **7** indicating a significant catalytic potential of simultaneous motion of both sliders on one deck (Figure 7).

Further, for both reactions in Scheme 1, the catalytic activity of the machinery shows a clear trend along **DS3**·NMP > **DS3′**·NMP > **DS3″**·NMP suggesting that the faster motion of both bipeds in **DS3** is relevant for the higher turnover (see Supporting Information, Figures S65 and S66).

In summary, we show an unprecedented case of synchronized motion using the five-component slider-on-deck system **DS3**, in which two very different sliding motions are kinetically coupled and result in synchronized movements despite a spatial separation of 2.2 nm. If the dual slider-on-deck **DS3** was treated with brake pads, both motions were slowed although the brake pad would only be able to affect the lutidine slider. An unmatched mechanism explaining the coupled motion and synchronization of speed via intercomponent communication, mimicking long-range communication in natural systems via the protein backbone-(s),[2] is provided. The mechanism conceptually has nothing at all in common with intimate steric interactions[14,28] or interdigitated geared motion[18,20,21] as in other man-made devices. Further, we have demonstrated how the coupling of both motions liberated two catalysts in high effective concentrations, a feature that was used to increase the yields in the double catalysis of benzofuran and indole products.

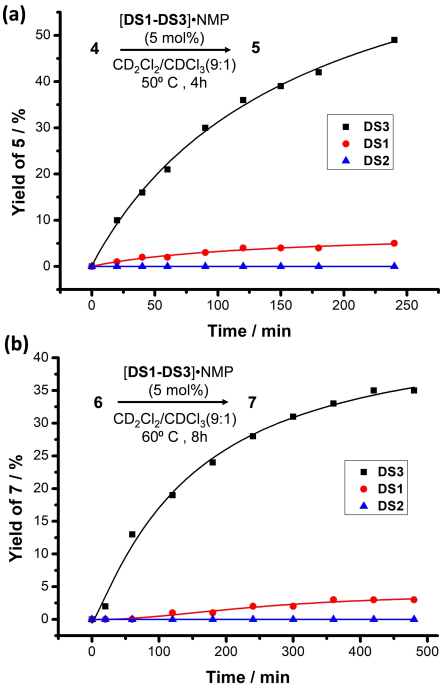

Figure 7. a) Results of the catalyzed reaction of **4**→**5** using 5 mol% of **DS1**–**DS3**. Kinetic evolution of product **5** over 4 h. b) Results of the catalyzed reaction of **6**→**7** using 5 mol% of **DS1**–**DS3**. Kinetic evolution of product **7** formation over 8 h.

Acknowledgements

We are grateful to the Deutsche Forschungsgemeinschaft (SCHM 647/22-1, No 491092614) and the University of Siegen for financial support. Open Access funding enabled and organized by Projekt DEAL.

Conflict of Interest

The authors declare no conflict of interest.

Data Availability Statement

The data that support the findings of this study are available from the corresponding author upon reasonable request.

Keywords: Catalytic Machinery · Double Catalysis · Kinetics · Multicomponent Device · Synchronized Motion

[1] P. K. Agarwal, *Biochemistry* **2019**, *58*, 438–449.
[2] H. Wang, G. Oster, *Nature* **1998**, *396*, 279–282.
[3] K. Adachi, K. Oiwa, T. Nishizaka, S. Furuike, H. Noji, H. Itoh, M. Yoshida, K. Kinosita, *Cell* **2007**, *130*, 309–321.
[4] C. Biagini, S. Di Stefano, *Angew. Chem. Int. Ed.* **2020**, *59*, 8344–8354; *Angew. Chem.* **2020**, *132*, 8420–8430.
[5] M. Baroncini, S. Silvi, A. Credi, *Chem. Rev.* **2020**, *120*, 200–268.
[6] A. Goswami, S. Saha, P. Biswas, M. Schmittel, *Chem. Rev.* **2020**, *120*, 125–199.
[7] S. Kassem, T. van Leeuwen, A. S. Lubbe, M. R. Wilson, B. L. Feringa, D. A. Leigh, *Chem. Soc. Rev.* **2017**, *46*, 2592–2621.
[8] S. Erbas-Cakmak, D. A. Leigh, C. T. McTernan, A. L. Nussbaumer, *Chem. Rev.* **2015**, *115*, 10081–10206.

[9] Y. Feng, M. Ovalle, J. S. W. Seale, C. K. Lee, D. J. Kim, R. D. Astumian, J. F. Stoddart, *J. Am. Chem. Soc.* **2021**, *143*, 5569–5591.
[10] C. Biagini, S. D. P. Fielden, D. A. Leigh, F. Schaufelberger, S. Di Stefano, D. Thomas, *Angew. Chem. Int. Ed.* **2019**, *58*, 9876–9880; *Angew. Chem.* **2019**, *131*, 9981–9985.
[11] L. van Dijk, M. J. Tilby, R. Szpera, O. A. Smith, H. A. P. Bunce, S. P. Fletcher, *Nat. Chem. Rev.* **2018**, *2*, 0117.
[12] I. Paul, A. Goswami, N. Mittal, M. Schmittel, *Angew. Chem. Int. Ed.* **2018**, *57*, 354–358; *Angew. Chem.* **2018**, *130*, 360–364.
[13] P. K. Biswas, S. Saha, T. Paululat, M. Schmittel, *J. Am. Chem. Soc.* **2018**, *140*, 9038–9041.
[14] N. N. Bach, V. Josef, H. Maid, H. Dube, *Angew. Chem. Int. Ed.* **2022**, *61*, e202201882; *Angew. Chem.* **2022**, *134*, e202201882.
[15] L.-S. Zheng, J.-S. Cui, W. Jiang, *Angew. Chem. Int. Ed.* **2019**, *58*, 15136–15141; *Angew. Chem.* **2019**, *131*, 15280–15285.
[16] V. V. Rajasekaran, I. Paul, M. Schmittel, *Chem. Commun.* **2020**, *56*, 12821–12824.
[17] K. Zhu, G. Baggi, S. J. Loeb, *Nat. Chem.* **2018**, *10*, 625–630.
[18] M. Nakamura, K. Kishimoto, Y. Kobori, T. Abe, K. Yoza, K. Kobayashi, *J. Am. Chem. Soc.* **2016**, *138*, 12564–12577.
[19] A. Goswami, M. Schmittel, *Angew. Chem. Int. Ed.* **2020**, *59*, 12362–12366; *Angew. Chem.* **2020**, *132*, 12461–12465.
[20] Y. Gisbert, S. Abid, C. Kammerer, G. Rapenne, *Chem. Eur. J.* **2021**, *27*, 12019–12031.
[21] I. Liepuoniute, M. J. Jellen, M. A. Garcia-Garibay, *Chem. Sci.* **2020**, *11*, 12994–13007.
[22] M. Schmittel, K. Mahata, *Chem. Commun.* **2010**, *46*, 4163–4165.
[23] M. Schmittel, *Chem. Commun.* **2015**, *51*, 14956–14968.
[24] N_{py}→ZnPor interaction: S. Liu, D. V. Kondratuk, S. A. L. Rousseaux, G. Gil-Ramirez, M. C. O'Sullivan, J. Cremers, T. D. W. Claridge, H. L. Anderson, *Angew. Chem. Int. Ed.* **2015**, *54*, 5355–5359; *Angew. Chem.* **2015**, *127*, 5445–5449.
[25] HETPYP interaction: M. L. Saha, J. W. Bats, M. Schmittel, *Org. Biomol. Chem.* **2013**, *11*, 5592–5595.
[26] E. Elramadi, A. Ghosh, I. Valiyev, P. K. Biswas, T. Paululat, M. Schmittel, *Chem. Commun.* **2022**, *58*, 8073–8076.
[27] The $\Delta G^{\neq}_{298}$ increase when going from **DS2** to **DS3** arises from a reduction of $\Delta S^{\neq}$, because departure of the pyr slider in **DS2** liberates all three arms of the deck, whereas in **DS3** only one arm is freely movable (the two others remain connected by the lut slider). In contrast, the $\Delta G^{\neq}_{298}$ reduction (for the lutidine sliding process) when going from **DS1** to **DS3** stems from the drastically reduced $\Delta H^{\neq}$.
[28] M. Kathan, S. Crespi, A. Troncossi, C. N. Stindt, R. Toyoda, B. L. Feringa, *Angew. Chem. Int. Ed.* **2022**, *61*, e202205801; *Angew. Chem.* **2022**, *134*, e202205801.

Manuscript received: August 24, 2022
Accepted manuscript online: October 5, 2022
Version of record online: October 26, 2022